Bumetanide-blocked SLC12A2 exerts a protective effect in experimental diabetic retinopathy

YUTING ZHANG[1,2*], XIULI WANG[3*], QINYUE XIE[4], YUE HUANG[1], DONGJIA HUANG[1], ZIQING LIU[1], TONG XU[1], MAN NI[5] and HONGWEI YANG[1,2]

[1]Department of Ophthalmology, Shengjing Hospital of China Medical University, Shenyang, Liaoning 110004, P.R. China; [2]The Second Affiliated Hospital of Shenyang Medical College, Shenyang, Liaoning 110002, P.R. China; [3]Department of Pediatrics, Shengjing Hospital of China Medical University, Shenyang, Liaoning 110004, P.R. China; [4]Department of Biochemistry, University of Illinois Urbana-Champaign, Urbana, IL 61801, USA; [5]Veterinary Medicine, Yangzhou University, Yangzhou, Jiangsu 225009, P.R. China

Received August 8, 2025; Accepted December 30, 2025

DOI: 10.3892/ijmm.2026.5774

Abstract. Diabetic retinopathy (DR) is a common microvascular complication that leads to vision loss in patients with diabetes. The SLC12A2/SLC12A4 inhibitor, bumetanide, has been reported to alleviate hypoxia-induced retinopathy. It was hypothesized that it may exert the same effect in DR. DR cell types and SLC12A2/SLC12A4 expression at the cell level were analyzed using single cell RNA-sequencing (scRNA-seq) data. Next, cell [high glucose (HG) stimulation] and animal (mice injected with streptozotocin) DR models were constructed. The protective effects and possible mechanisms of bumetanide and SLC12A2 were investigated through a series of experiments, including Cell Counting Kit-8, TUNEL, Transwell, tube formation, ELISA, immunofluorescence staining, western blot and reverse transcription-quantitative PCR assays. Bumetanide reduced HG-induced cell apoptosis by suppressing the expression of SLC12A2 and SLC12A4. Second, scRNA-seq analysis revealed that SLC12A2 was predominantly expressed in endothelial cells, which are the main targets of hyperglycemic damage. Endothelial cell-related markers were involved in angiogenesis and adhesion molecule-related pathways. Third, in HG-stimulated cells, SLC12A2 knockdown efficiently reduced the inflammatory response and angiogenesis, while maintaining endothelial barrier integrity. This protective process involved reduced release of inflammatory factors (IL-1β and IL-6) and growth factors (vascular endothelial growth factor), suppression of adhesion molecule expression (VCAM1, ICAM1, E-Selectin and P-Selectin), activation of tight junction protein (ZO-1), and decreased matrix metalloproteinases (MMP2 and MMP9). Furthermore, SLC12A2 deficiency ameliorated DR progression in streptozotocin-induced diabetic mice by improving retinal thickness and pathological changes. The present study elucidates the crucial role of bumetanide in DR treatment and suggests that targeting SLC12A2 may represent a novel therapeutic strategy for the prevention of DR.

Correspondence to: Dr Hongwei Yang, Department of Ophthalmology, Shengjing Hospital of China Medical University, 36 Sanhao Street, Heping, Shenyang, Liaoning 110004, P.R. China
E-mail: yanghw@sj-hospital.org

*Contributed equally

Key words: diabetic retinopathy, bumetanide, SLC12A2, SLC12A4, single-cell transcriptomics

Introduction

Diabetic retinopathy (DR), a widespread microvascular complication of diabetes, is a progressive disease and a leading cause of vision loss (1). With the increasing prevalence of diabetes, the number of patients with DR is rapidly increasing. The global incidence of DR is projected to reach 160.5 million by 2045, increasing the demand for ophthalmic care and treatment (2). Currently, treatment strategies for DR are limited to advanced cases presenting with symptoms of retinal damage, and mainly include laser photocoagulation, surgery and intravitreal injections of anti-vascular endothelial growth factor (VEGF) or corticosteroids (3). Although these methods can restrict disease progression, they do not prevent side effects or treatment resistance. Considering that most DR are preventable, there is an urgent need to find new ways to treat DR. In recent years, the identification of specific biomarkers can provide a scientific basis for the development of DR therapeutic agents, such as RBP3 (4,5). However, the targets available for clinical use are still lacking.

Bumetanide (PubChem CID: 2471) is a potent circulating diuretic that acts by inhibiting Na-K-Cl co-transport and is effective in the treatment of various inflammations or ischemia-induced edema (6). Recent evidence has uncovered the potential role of bumetanide in the alleviation of retinopathy. For example, it exhibits antiangiogenic and oxidative stress inhibitory properties in oxygen-induced retinopathy (7). It also reduced the number of apoptotic cells and the expression of AQP4 (a factor involved in retinal edema) in a retinal ischemia-reperfusion injury (8). In addition, bumetanide has anti-inflammatory properties and low cytotoxicity, which suppresses diabetic activity (9). However, it is unclear whether

bumetanide has effect in attenuating DR. To the best of the authors' knowledge, the pharmacological effects of bumetanide involve the modulation of NKCC1 (also known as SLC12A2) and KCC2 (also known as SLC12A4) (10,11). Moreover, there is a large gap regarding the influence of SLC12A2 and SLC12A4 on the pathophysiology of DR.

The emergence of single-cell RNA sequencing (scRNA-seq) technology has provided an opportunity to dissect complex pathological mechanisms at single-cell resolution (12). In 2020, Van Hove *et al* (13) first applied scRNA-seq in DR to reveal the cellular and molecular changes of the disease (13). Since then, an increasing number of studies have used scRNA-seq, which can be considered a powerful tool for developing effective therapeutic targets, to explore the underlying mechanisms of DR (14). Reportedly, dysfunction of some endothelial cell subpopulations (specifically expressing IL-1β, S100A8, S100A9) during DR enhanced the release of inflammatory molecules and stimulation of adhesion molecules, leading to increased neovascularization and permeability (15). The elimination of functional endothelial cell subpopulations may delay the progression of DR. Hence, scRNA-seq has great potential for identifying new therapeutic strategies for DR.

In the present study, bioinformatics analysis and biological approaches were employed to elucidate the protective effects of bumetanide against DR and its underlying mechanisms. A flow chart and the experimental design are depicted in Fig. 1. It was demonstrated that SLC12A2 and SLC12A4 play critical roles in mediating the protective effects of bumetanide. Subsequently, utilizing scRNA-seq and RNA-seq data from the Gene Expression Omnibus (GEO; https://www.ncbi.nlm.nih.gov/geo/) database, it was found that SLC12A2 was highly expressed in endothelial cells, which are the primary targets of hyperglycemic damage (16). Endothelial cell markers were enriched in the angiogenesis regulation and adhesion molecule-related pathways. *In vitro* and *in vivo* experiments further revealed that under hyperglycemic conditions, SLC12A2 deficiency reduced endothelial cell apoptosis and inflammatory events by inhibiting cell adhesion molecules, thereby contributing to improved DR. These findings provide novel insights into the role of bumetanide in DR and its regulatory genes, highlighting SLC12A2 as a promising therapeutic target for DR.

Materials and methods

Bioinformatics analysis

Research datasets. DR-related datasets were retrieved from the GEO database using the keyword 'DR'. Ultimately, five datasets were selected for the present study. Among them, there were three scRNA-seq datasets [GSE165816 (17); 3 healthy samples; GSE248284 (18); 3 DR cases; GSE165784 (19); 5 DR cases] and two RNA-seq datasets [GSE221521 (20); 69 DR and 50 healthy; and GSE185011 (21); 5 DR and 5 healthy].

scRNA-seq data processing. First, data from the three scRNA-seq datasets were merged using Seurat (version 4.4.0) in the R package (version 4.3.3; https://cran.r-project.org/), and low-quality cells were removed, including those with gene counts <500, mitochondrial genes >25%, and erythrocyte genes >3%. Second, after normalizing the data with NormalizeData, FindVariableFeatures was utilized to extract intercellular variable genes, and 2,000 highly variable genes were screened for analysis. The RunPCA function was applied to conduct principal component analysis of the cells based on the expression levels of the variable genes, and the top 20 PC with statistical significance were selected for downstream analysis. Next, the cells were analyzed by t-distributed Stochastic Neighbour Embedding (t-SNE) non-linear dimensionality reduction using the FindCluster tool. Finally, marker genes for each cell cluster were identified by the Seurat package, followed by the annotation of cells using CellMarker. Notably, the distribution of the key genes, SLC12A2 and SLC12A4, was also demonstrated in different cells using t-SNE maps.

Functional enrichment analysis. As both scRNA-seq analysis and literature reports indicate the key role of endothelial cells in the pathogenesis of DR, the major functions of the marker gene set were explored in endothelial cells (22). Specifically, the top 200 marker genes of endothelial cells were included in Gene Ontology (GO; https://geneontology.org/) and Kyoto Encyclopedia of Genes and Genomes (KEGG; https://www.genome.jp/kegg/) enrichment analyses.

Experimental procedures

Cell culture. Rat retinal microvascular endothelial cells (RRMECs; cat. no. CP-R114) and 293T cells (cat. no. CL-0005) obtained from Pricella Biotechnology Co., Ltd. were cultured in DMEM [containing 10% FBS (cat. no. 26-500-FBS; Ephraim), 1% penicillin/streptomycin] and a humid atmosphere at 37˚C/5% CO_2. RRMECs were exposed to normal glucose (5 mM) or high glucose (HG, 25 mM, simulating an *in vitro* DR model) (23).

Cell treatment. In the present study, two experiments were designed to explore the effects of bumetanide and SLC12A2 on cells. In experiment 1, the cells were classified into control, HG, and HG + Bumetanide groups. For drug treatment, cells were treated with 10 μM of bumetanide in the presence of HG for 24 h at 37˚C.

In experiment 2, the cells were classified into control, HG, HG + sh-NC and HG + sh-SLC12A2 groups. Specific targeting of SLC12A2 (sh-SLC12A2, 5'-CCAAGTTCTTCT TACATTATA-3') and negative control (sh-NC, 5'-CCTAAG GTTAAGTCGCCCTCG-3') sequences were designed by using VectorBuilder platform (VectorBuilder Inc.). For the NC and sh-SLC12A2 groups, 12 μg target plasmid (sh-NC or sh-SLC12A2) and 12 μg packaging plasmids (pMDLg/pRRE: pVSV-G: pRSV-Rev=5:3:2) were transfected into 293T cells using 8 μl HighGene reagent (cat. no. RM09014; ABclonal Biotech Co., Ltd.). After 48 and 72 h of transfection (at 37˚C), the supernatant containing the virus was collected separately for transduction of target cells (RRMECs). The collected supernatants were mixed and centrifuged at 3,000 x g for 10 min at 4˚C, and then filtered through a 0.45-μm membrane. During transduction, lentiviral solution with a titer of $1x10^8$ TU/ml was added to well-growing RRMECs (cell density 70-90%; multiplicity of infection=20), and cells were infected for 18 h at 37˚C. Subsequently, the viral medium was replaced with fresh medium. After continuing the transduction for 72 h, the cells were selected using 2.5 μg/ml puromycin. Stable SLC12A2 knockdown cell line was established following 1 week of selection culture. Cells were then expanded in medium containing puromycin at a reduced concentration of

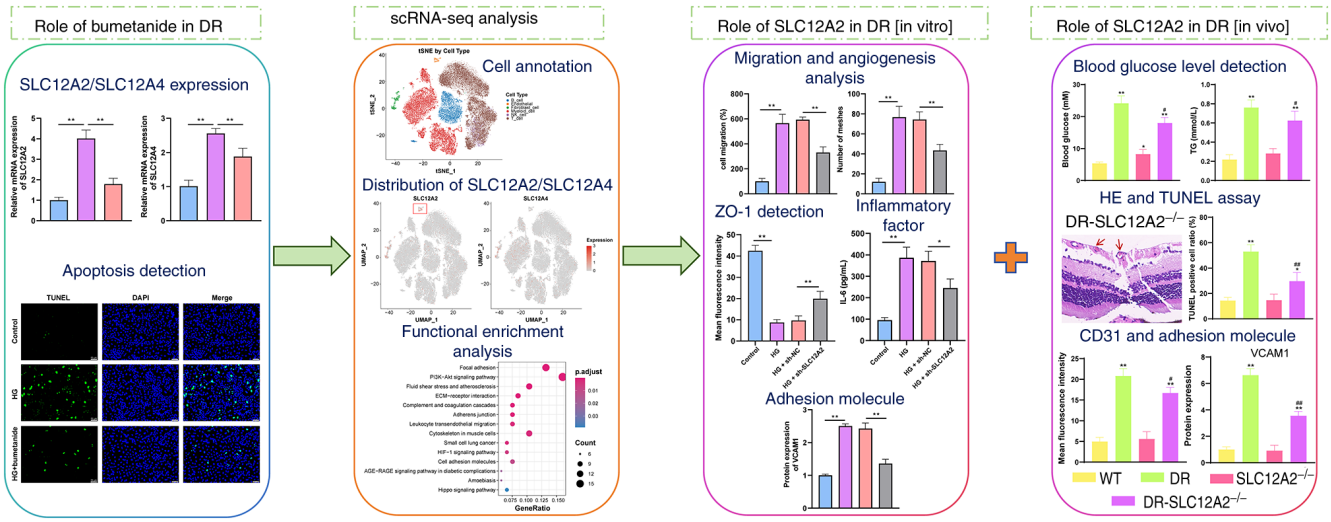

Figure 1. Design flow chart of the present study. DR, diabetic retinopathy.

0.67 μg/ml. Reverse transcription-quantitative PCR (RT-qPCR) and western blotting were performed 1 week after initiation of this expansion phase to examine knockdown efficiency. After confirming SLC12A2 knockdown, cells were seeded in HG (25 mM) medium for 24 h.

Cell viability assessment. Cell viability was measured via Cell Counting Kit-8 (CCK-8) (24). After transfection for 24 h, CCK-8 reaction solution (10 μl; cat. no. C0037; Beyotime Institute of Biotechnology) was added to each well and incubated for 2 h at 37˚C. Cell viability was expressed as the absorbance at 450 nm measured by the enzyme labeler (cat. no. DR-3518G; Hiwell-Diatek Instruments Co., Ltd.).

Cell migration evaluation. Transwell was used to assess the cell migratory capacity of cells (25). In brief, 200 μl of cell suspension was added to the Transwell chamber (8-μm pore size) at a density of 1x10^5/ml, while medium (containing 10% FBS) was added at the bottom chamber, maintaining in the incubator for 24 h. Next, the cells were fixed with methanol [30 min, room temperature (RT)] and stained with 0.1% crystal violet (20 min, RT). After swabbing the non-migratory cells, three fields were randomly selected for observation and calculation of the number of migratory cells under a light microscope (magnification, x200).

Tube formation test. Tube formation test was performed according to a previous study (26). After trypsin digestion and re-suspension, cell suspensions were seeded into 24-well plates coated with Matrigel gel with a density of 5x10^4/well and then incubated for 72 h. Matrigel was polymerized at 37˚C for 30 min before cell seeding. After that, images of three fields were randomly selected to be captured with a microscope (magnification, x100), and the number of meshes was quantified with ImageJ software (National Institutes of Health).

Inflammatory factor detection. The secretion levels of VEGF (cat. no. ml002862), IL-1β (cat. no. ml037361), IL-6 (cat. no. ml102828) and TNF-α (cat. no. ml002859; all from Shanghai Enzyme-linked Biotechnology Co., Ltd.) in cell supernatant were estimated using commercial kits, in accordance with the instructions.

ZO-1 detection. Changes in ZO-1 expression were evaluated by immunofluorescence (IF) staining to reveal the permeability of the blood-retinal barrier (BRB) (27). After fixation with formaldehyde (4%, 15 min, RT) and permeabilization with Triton-X (1%), the cells were blocked with a BSA solution (3%, 30 min, RT; Beijing Solarbio Science & Technology Co., Ltd.). Subsequently, samples were incubated with ZO-1 primary antibody (cat. no. AF5145; Affinity Biosciences) at 4˚C overnight and then reacted with fluorescent Alexa Fluor® 488-conjugated goat anti-rabbit IgG H&L secondary antibody (1:500, dilution; cat. no. ab150077; Abcam)/DAPI (0.001 mg/ml) mixture for 30 min. Cell images were captured using a fluorescence microscope.

Matrix metalloproteinases (MMPs) examination. MMPs regulate various pathological processes and can lead to the breakdown of tight junction proteins such as ZO-1 under HG stimulation, thus destroying the integrity of the BRB (28). In the present study, kits for MMP2 (cat. no. E-EL-R0618) and MMP9 (cat. no. E-EL-R3021; both from Elabscience Biotechnology, Inc.) were employed to detect the activity of these two factors in cell supernatants. The experiments were performed according to the manufacturer's instructions.

Animal model establishment and grouping. Animal experiments utilized 20 C57BL/6 (wild-type, WT) and 20 SLC12A2$^{-/-}$ C57BL/6 (SLC12A2 specific knockout, SLC12A2-KO) mice (age, 6 weeks; weight, 18-22 g), with equal numbers of males and females (n=10 per sex) in each genotype group. Genotyping of the mice was determined by PCR amplification. Animal treatments followed the ARVO Statement for the Use of Animals in Ophthalmic and Vision Research. All animal experiments were conducted at Yangzhou University and were approved by the Animal Care and Use Committee of Yangzhou University (approval no. 202410027; Yangzhou, China). WT mice were randomly divided into two groups: control (WT) and diabetic (DR). Similarly, SLC12A2-KO mice were classified into control

(SLC12A2$^{-/-}$) and diabetic (DR-SLC12A2$^{-/-}$) groups. There were 10 mice in each group. All mice were housed in a pathogen-free facility with standard conditions (circadian pattern: light hours 6:00-18:00; temperature: 22-24˚C; humidity: 30-50%). As described previously (29), DR and DR-SLC12A2$^{-/-}$ mice were intraperitoneally injected with STZ (50 mg/kg) for 7 consecutive days. For the control groups (WT and SLC12A2$^{-/-}$), mice were intraperitoneally injected with the same volume of citrate buffer. At the end of the treatment, the body weight of the mice was recorded. Meanwhile, blood glucose was measured at the tail by a glucose meter (OneTouch Verio Vue, Johnson & Johnson Medical (China) Ltd.). Mice with blood glucose levels greater than 16.7 mmol/l were considered diabetic mice for the study. Venous blood (tail vein) was collected to evaluate the glucolipid metabolism of mice. Subsequently, the mice were deeply anesthetized by intraperitoneal injection of 2% sodium pentobarbital (40 mg/kg), followed by euthanasia via cervical dislocation. Death was confirmed by the absence of a heartbeat and spontaneous respiration. The retinal specimens were collected for further experiments.

Detection of blood biochemical indexes. Venous blood was centrifuged at 1,000 x g, 4˚C for 15 min, and serum samples were harvested. The concentrations of triglyceride (TG), total cholesterol (TC), low-density lipoprotein cholesterol (LDL-C), high-density lipoprotein cholesterol (HDL-C) and glycated hemoglobin (HbA1c) in serum were determined using a biochemical autoanalyzer (30). Moreover, commercial Enzyme-linked immunosorbent assay (ELISA) kits were applied to detect the levels of serum inflammatory factors, including VEGF (cat. no. PV957), IL-1β (cat. no. PI301), IL-6 (cat. no. PI326) and TNF-α (cat. no. PT512; all from Beyotime Institute of Biotechnology), followed by quantification of the concentrations by measuring absorbance with a microplate reader. All experiments were conducted following the manufacturer's provided protocol.

Hematoxylin and eosin (H&E) staining. H&E staining was utilized to assess the pathological changes in the retina, including ganglion cell layer (GCL), inner plexiform layer, inner nuclear layer (INL), outer plexiform layer and outer nuclear layer (ONL) (31). Briefly, retinal samples were fixed in 4% paraformaldehyde at RT for 24 h, dehydrated with an ethanol gradient, and embedded in paraffin. Slices with a thickness of 5 μm were cut from the sample on a microtome, and then H&E staining was performed according to the standard procedures (32). Structural changes in the tissue were observed under a light microscope, and retinal thickness was quantified.

Apoptosis assay. Terminal deoxynucleotidyl transferase dUTP nick-end labeling (TUNEL) approach was employed to assess apoptosis status (33). For *in vitro* observation, cells and nuclei were stained with TUNEL (cat. no. C1082; 60 min, 37˚C) and DAPI (cat. no. C1005; both from Beyotime Institute of Biotechnology; 10 min, RT) reagents. For tissue detection, retinal sections were deparaffinized/rehydrated, treated with proteinase K for 30 min, and then washed three times with PBS. Afterwards, the tissue sections were stained successively with TUNEL (60 min, 37˚C) and DAPI (0.001 mg/ml, 10 min, RT) reagents. Finally, the staining of cells or tissue sections was observed under a fluorescence microscope. Among them, blue and green fluorescence represented nuclei and TUNEL-positive cells, respectively.

CD31 measurement. To evaluate pathological changes in blood vessels, the IF method was employed to detect the expression levels of CD31, a specific marker for vascular endothelial cells (34). Retinal sections were incubated with primary antibody anti-CD31 (cat. no. ab222783; Abcam) overnight at 4˚C. After washing with PBS, the samples were incubated with secondary antibody for 1 h at 37˚C, followed by staining of nuclei with DAPI (0.001 mg/ml). Fluorescence images were captured by confocal fluorescence microscopy.

RT-qPCR. RT-qPCR assay was undertaken as previously described (35). Total RNA from cells or retinal tissues was prepared by using TRIzol (cat. no. 15596018CN; Thermo Fisher Scientific, Inc.), followed by reverse transcription to cDNA using FastKing RT SuperMix (cat. no. KR118-02; Tiangen Biotech Co., Ltd.) according to the manufacturer's protocol. The mRNA was quantified using SYBR Green PCR Master Mix (cat. no. A4004M; Xiamen Life Internet Technology Co., Ltd.) and a Real-time PCR system (cat. no. CFX96 Touch; Bio-Rad Laboratories, Inc.). RT-qPCR was conducted under the following thermocycling conditions: An initial denaturation at 95˚C for 10 min, followed by 40 cycles of denaturation at 95˚C for 12 sec, and annealing/extension at 60˚C for 40 sec. Finally, the relative gene expression was calculated via $2^{-\Delta\Delta cq}$ (36), with GAPDH as a stable reference. The primer sequences are displayed in Table SI.

Western blot analysis. Western blot analysis was conducted as previously described (35). Briefly, total protein was collected from cultured cell or retinal tissues using RIPA lysis buffer (cat. no. P0013B; Beyotime Institute of Biotechnology), and protein concentration was determined by using the BCA assay. The proteins (25 μg) separated by electrophoresis were transferred to PVDF membrane and blocked by skim milk powder (5%) for 60 min at RT. Furthermore, the membranes were incubated overnight with the primary antibody at 4˚C and continued incubation with goat anti-rabbit IgG for 60 min at RT. The bands were developed with ECL reagent (cat. no. P1000; Applygen Technologies, Inc.), and the gray values were quantified with ImageJ software (version 1.53k; National Institutes of Health). All western blot data were normalized to GAPDH. Detailed information on the antibodies used is provided in Table SII.

Statistics. Statistical analyses were done using R (version 4.3.3; bioinformatics analysis) or GraphPad Prism (version 8.0; Dotmatics; experimental section). Measurement data were exhibited as the mean ± SD, with experiments replicated at least three times. Group differences were analyzed using one-way analysis of variance (ANOVA) followed by Tukey's multiple comparison post-test. $P<0.05$ was considered to indicate a statistically significant difference.

Results

Bumetanide mitigates SLC12A2, SLC12A4 and apoptosis in HG-treated RRMECs. Considering the protective effects of

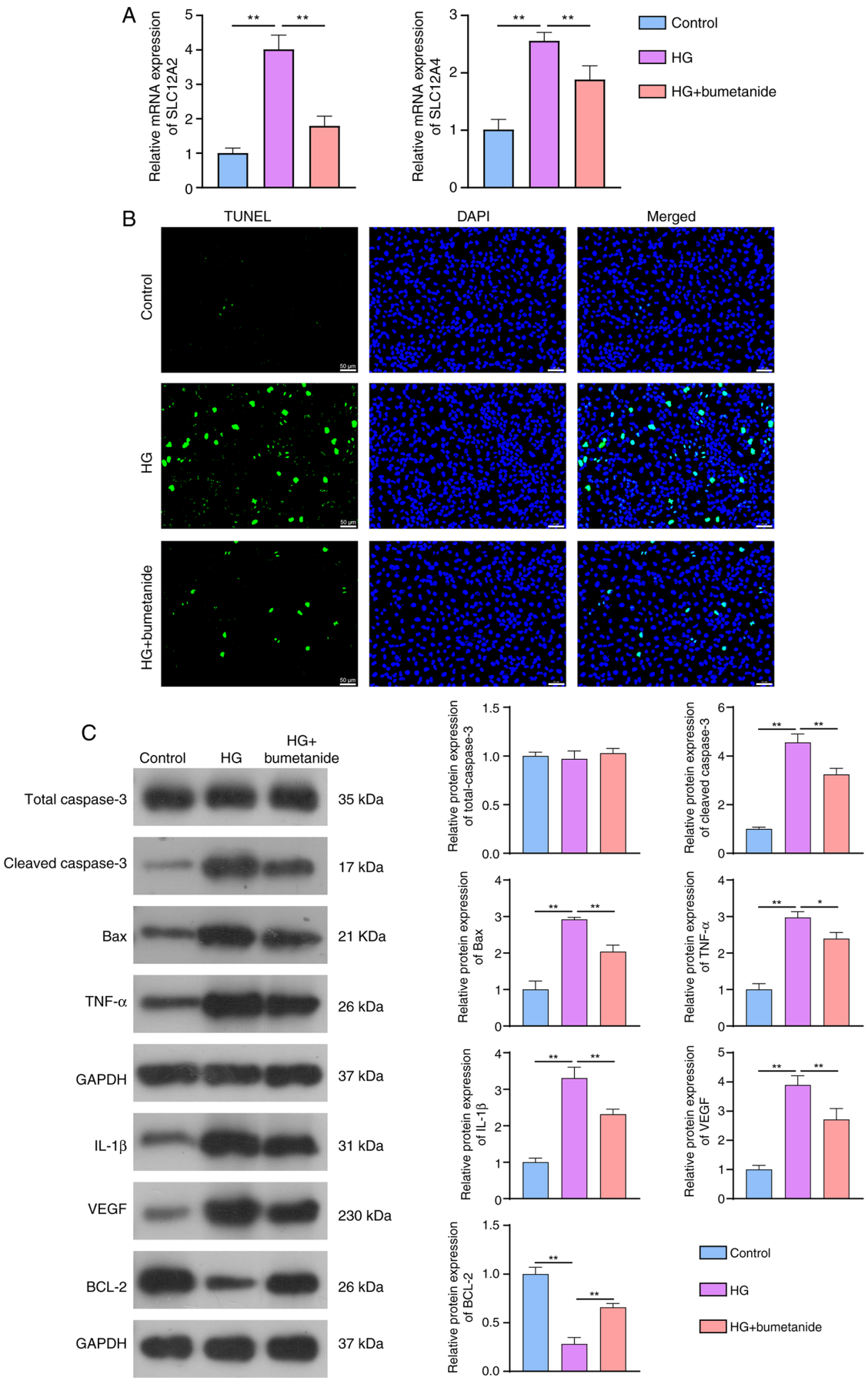

Figure 2. Bumetanide alters SLC12A2/SLC12A4 expression levels and apoptosis in HG-treated rat retinal microvascular endothelial cells. (A) Expression levels of SLC12A2 and SLC12A4 detected by reverse transcription-quantitative PCR. (B) Cell apoptosis in different groups assessed by TUNEL assay. (C) Expression levels of apoptosis-related proteins measured by western blot. Data from three independent experiments are indicated as the mean ± SD (n=3). *P<0.05 and **P<0.01. HG, high glucose; TUNEL, terminal deoxynucleotidyl transferase dUTP nick-end labeling.

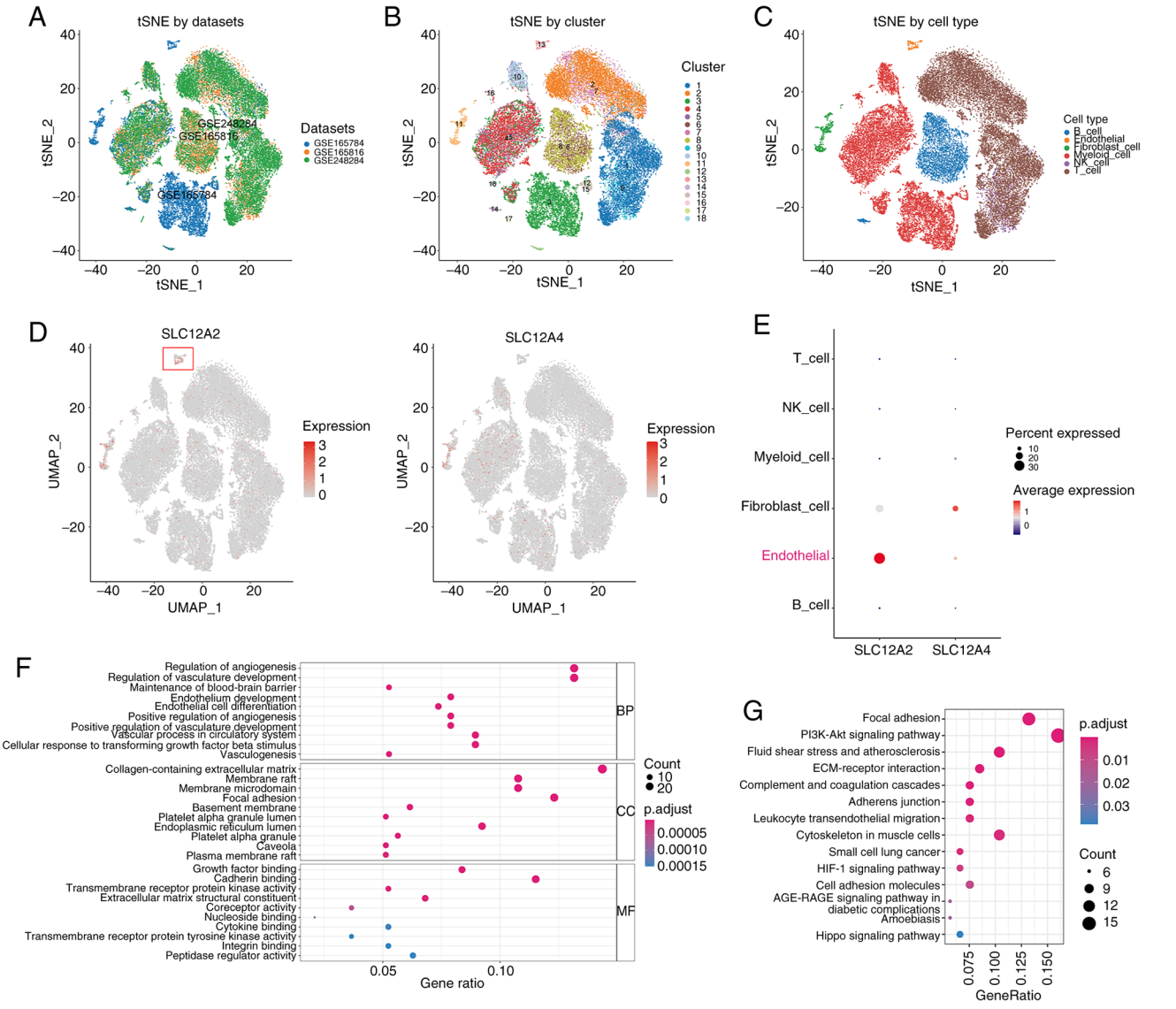

Figure 3. Results of single-cell RNA sequencing analysis. (A) t-SNE plot of samples from different datasets after dimensionality reduction. (B) t-SNE plot of 38,744 cells isolated from the samples, showing the 18 identified clusters. (C) t-SNE plot displaying the final annotation of the six known cell types in the samples. (D) UMAP plot and (E) global expression levels of SLC12A2 and SLC12A4. (F) Gene Ontology terms and (G) Kyoto Encyclopedia of Genes and Genomes pathway analyses of the top 200 endothelial cell markers. t-SNE, t-distributed Stochastic Neighbor Embedding; UMAP, uniform manifold approximation and projection.

bumetanide against retinopathy, the expression levels of these two genes were determined using RT-qPCR. Results showed that the mRNA expression levels of SLC12A2 and SLC12A4 in the HG group were obviously increased compared with those in the control group. However, bumetanide treatment significantly reduced their expression compared with that in the HG (Fig. 2A). Retinal cell apoptosis is an early feature of DR (37), and apoptosis-related indices were measured. TUNEL staining indicated that apoptosis was more serious in the HG group than in the control group; however, it was significantly alleviated in the HG group after treatment with bumetanide (Fig. 2B). Afterwards, western blotting was conducted to examine the expression of apoptotic proteins. Compared with the HG group, bumetanide significantly suppressed protein expression levels of cleaved-caspase 3, Bax, TNF-α, IL-1β and VEGF, while promoting BCL-2 protein expression, with no significant alteration in the total caspase 3 level (Fig. 2C). Taken together, bumetanide reversed retinal cell apoptosis, and its therapeutic effects involved the modulation of SLC12A2 and SLC12A4 expression.

Single-cell landscapes. The three scRNA seq datasets used in the present study were obtained from the GEO database. After quality control and filtering of the data, 38,744 cells and 21,412 genes were identified. Next, the three datasets were analyzed using downscaling and de-batching. The samples from the different datasets were well integrated without a significant batch effect, making them suitable for subsequent cluster analysis (Fig. 3A). The top 2,000 highly variable genes were selected for downstream analysis. Cluster analysis of the cells was performed using the Seurat package, and 18 cell clusters were obtained. Results were visualized by using a t-SNE diagram (Fig. 3B). From these clusters, the following six known cell types were identified with reference to cell type

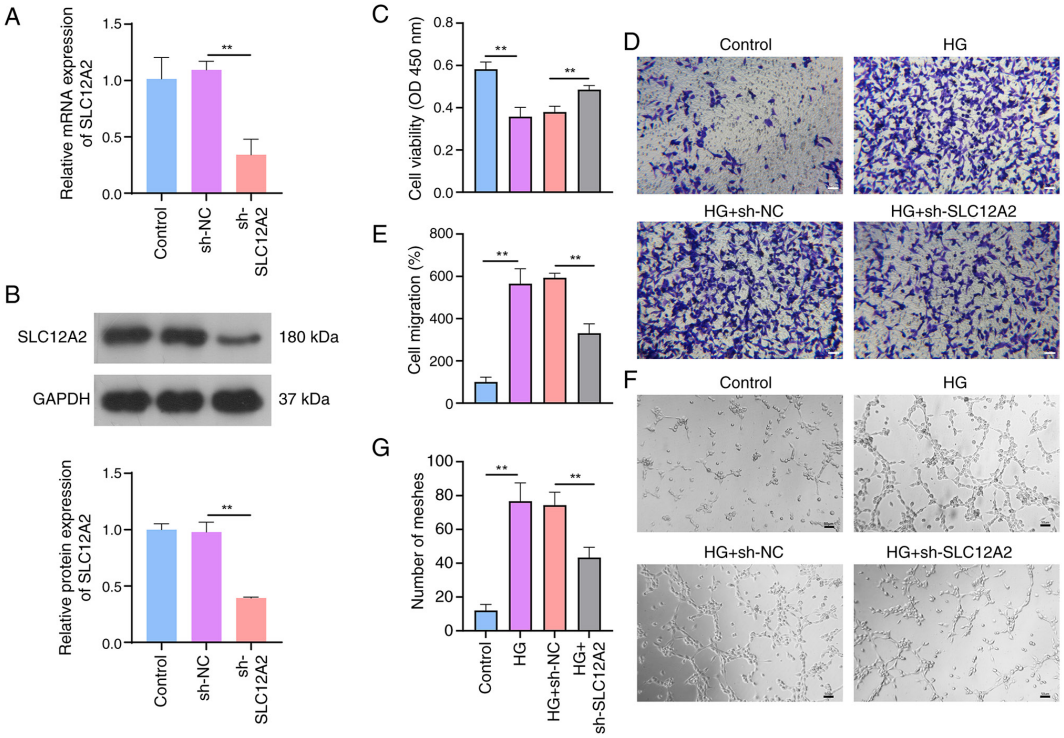

Figure 4. Effect of SLC12A2 knockdown on cell migration and angiogenesis in HG-treated RRMECs. (A and B) RRMECs were transfected with sh-NC or sh-SLC12A2; the SLC12A2 expression levels were detected by (A) reverse transcription-quantitative PCR and (B) western blot assays. (C) Cell viability of RRMECs in different treatments was measured by Cell Counting Kit-8 at 24 h. (D and E) Migration ability of RRMECs in different treatments was assessed by Transwell and its quantitative results. (F and G) Tube formation ability of RRMECs in different treatments and quantification of mesh number. Data from three independent experiments are indicated as the mean ± SD (n=3). **P<0.01. HG, high glucose; RRMECs, rat retinal microvascular endothelial cells; sh-, short hairpin; NC, negative control.

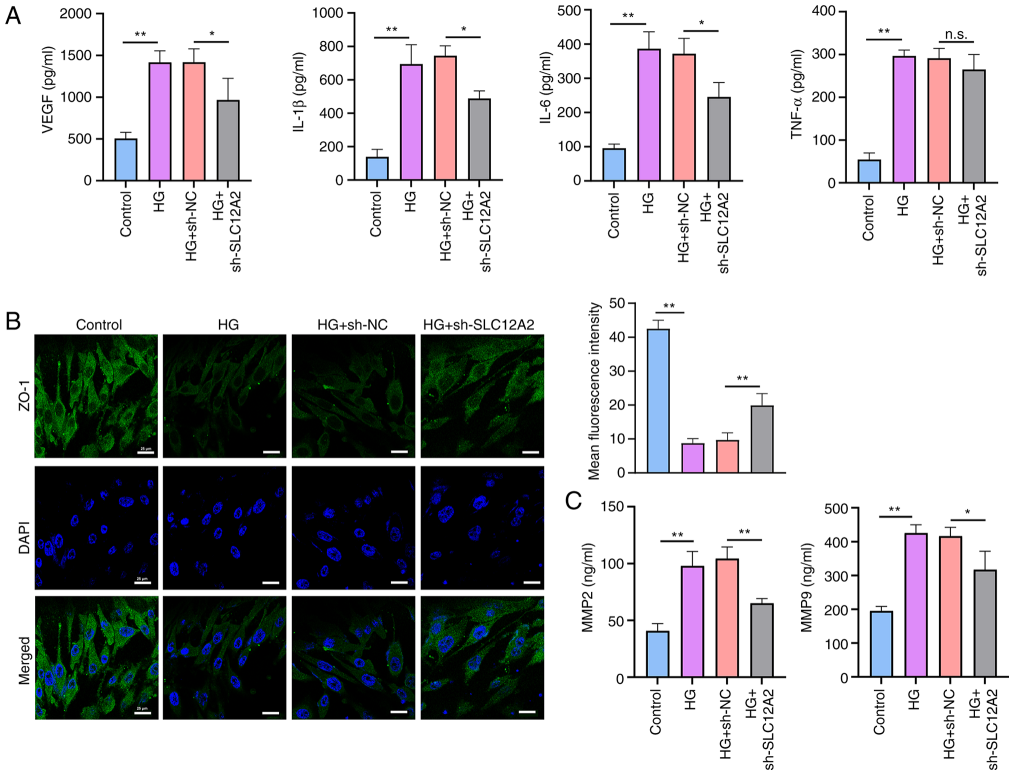

Figure 5. Effect of SLC12A2 knockdown on inflammatory factor release and blood-retinal barrier in HG-treated rat retinal microvascular endothelial cells. (A) Levels of VEGF, IL-1β, IL-6 and TNF-α detected by ELISA. (B) Immunofluorescence staining showing the ZO-1 expression in each group. (C) Levels of MMP2 and MMP9 detected by commercial kits. Data from three independent experiments are indicated as the mean ± SD (n=3). *P<0.05 and **P<0.01. HG, high glucose; VEGF, vascular endothelial growth factor; IL-1β, interleukin-1Beta; IL-6, interleukin-6; TNF-α, tumor necrosis factor-alpha; ZO-1, zonula occludens-1; MMP, matrix metalloproteinase; n.s., not significant.

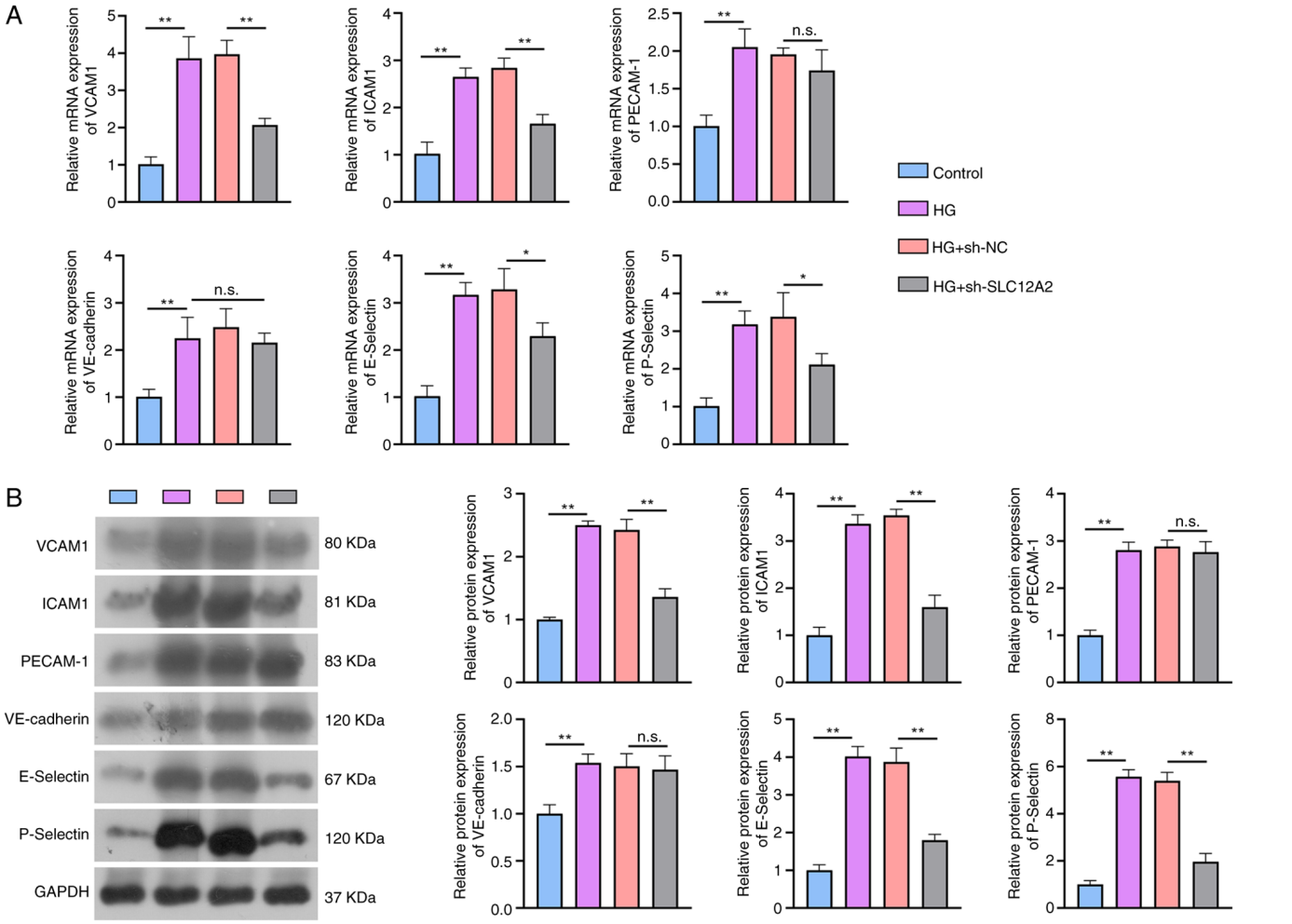

Figure 6. Effect of SLC12A2 knockdown on adhesion molecules in HG-treated rat retinal microvascular endothelial cells. (A) Reverse transcription-quantitative PCR and (B) western blot assays for expression levels of adhesion molecules, including VCAM1, ICAM1, PECAM-1, VE-cadherin, E-Selectin and P-Selectin. Data from three independent experiments are indicated as the mean ± SD (n=3). *P<0.05 and **P<0.01. HG, high glucose; VCAM1, vascular cell adhesion molecule-1; ICAM1, intercellular adhesion molecule-1; PECAM-1, platelet endothelial cell adhesion molecule-1; VE, vascular endothelial; sh-, short hairpin; NC, negative control.

marker genes recorded in the cell marker database: T cells, NK cells, B cells, myeloid cells, endothelial cells and fibroblast cells (Fig. 3C).

Next, focus was addressed on the expression distribution of the key genes SLC12A2 and SLC12A4 in different cells. Results revealed that SLC12A2 was mainly enriched in endothelial cells, whereas SLC12A4 expression was enhanced in fibroblast cell clusters (Fig. 3D and E). Microvascular endothelial cells are the main targets of hyperglycemic damage in the pathological microenvironment of diabetes. Retinal endothelial cell dysfunction is closely associated with DR (16). Hence, the functional enrichment analysis of the top 200 marker genes in endothelial cells was performed. GO analysis indicated that these genes were primarily enriched in regulation of angiogenesis (GO-BP), collagen-containing extracellular matrix (GO-CC) and cadherin binding (GO-MF) (Fig. 3F). Furthermore, KEGG enrichment analysis suggested that these genes were involved in adhesion molecule-related pathways, such as focal adhesion, adherens junction and cell adhesion molecules (Fig. 3G). Overall, the contribution of SLC12A2 and endothelial cells to DR pathology deserves further exploration.

Knockdown of SLC12A2 alleviates HG-induced abnormal migration and angiogenesis of HG-induced RRMECs. To explore the engagement of SLC12A2 in the cell model, RRMECs with SLC12A2 knockdown were generated via lentiviral delivery of short hairpin RNA (Fig. 4A and B). Under HG conditions, CCK-8 analysis indicated that the viability of RRMECs was significantly reduced; however, the cell activity was restored after SLC12A2 knockdown (Fig. 4C). Cell migration and the number of meshes were also measured. Exposure to HG increased the number of migratory RRMECs, which was attenuated by the SLC12A2 knockdown (Fig. 4D and E). HG observably enhanced the tube-forming capacity of cells, but this effect was weakened by downregulation of SLC12A2 (Fig. 4F and G). Overall, SLC12A2 knockdown protected cells from HG damage.

Knockdown of SLC12A2 inhibits inflammatory factors and restores retinal endothelial barrier function in HG-treated RRMECs. The pathophysiological mechanisms of DR are complex and involve the increased secretion of VEGF and pro-inflammatory mediators (38). As previously reported, significant increases in VEGF and inflammatory factors

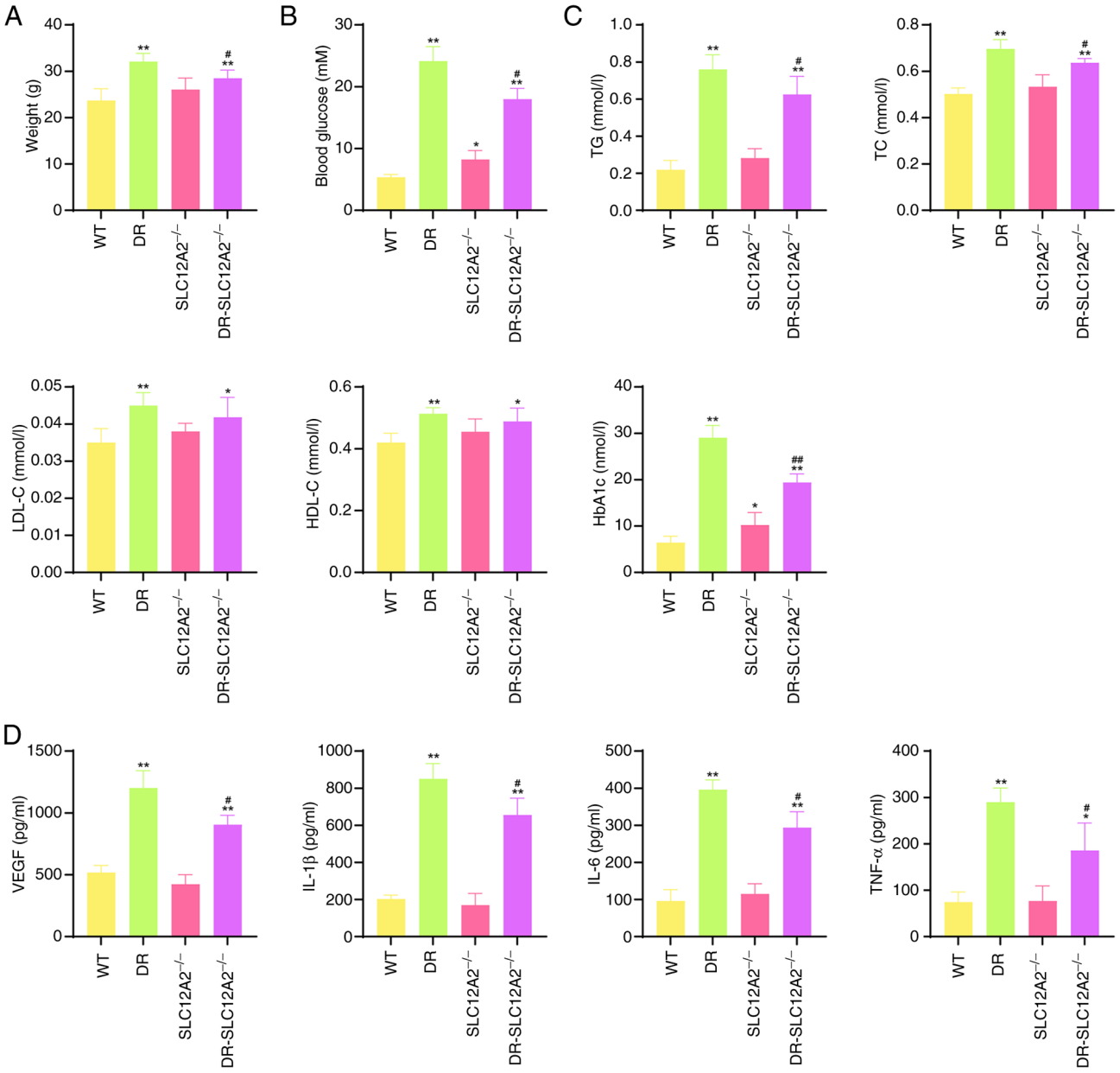

Figure 7. SLC12A2 deficiency ameliorates hyperglycemic and inflammatory effects in streptozotocin-induced diabetic mice. (A) Body weight and (B) blood glucose levels of mice at the end of the experiment. (C) Serum lipid and HbA1c levels of all mice. (D) Levels of inflammatory factors (VEGF, IL-1β, IL-6 and TNF-α) detected by commercial ELISA kits. Results are expressed as the mean ± SD (n=10/group). *P<0.05 and **P<0.01 vs. the WT group; $^{\#}$P<0.05 and $^{\#\#}$P<0.01 vs. the DR group. HbA1c, glycated hemoglobin; VEGF, vascular endothelial growth factor; IL-1β, interleukin-1Beta; IL-6, interleukin-6; TNF-α, tumor necrosis factor-alpha; WT, wild-type; TG, triglyceride; TC, total cholesterol; LDL-C, low-density lipoprotein cholesterol; HDL-C, high-density lipoprotein cholesterol; DR, diabetic retinopathy.

(IL-1β, IL-6 and TNF-α) were also observed in the HG group, which were ameliorated by SLC12A2 knockdown (Fig. 5A). ZO-1 is a tight connexin, and its abnormality can disrupt the BRB and increase the permeability of the retinal vasculature (39). Additionally, MMPs are involved in BRB disruption in DR. Therefore, the effect of SLC12A2 knockdown on these indicators was explored. As demonstrated in Fig. 5B and C, compared with the control group, the fluorescence intensity of ZO-1 was significantly inhibited in the HG group, while the levels of MMP2 and MMP9 were enhanced. Notably, the aberrant expression of ZO-1 and MMP2/9 in HG was clearly reversed after SLC12A2 knockdown.

Knockdown of SLC12A2 suppresses the expression of cell adhesion-related molecules in HG-treated RRMECs. Cell adhesion molecules have been found to be involved in the regulation of diseases in scRNA-seq analyses, and have been reported to be positively correlated with DR severity (40). Thus, the regulatory role of SLC12A2 in cell adhesion-related molecules was confirmed. Compared with the control group, HG treatment caused a distinct upregulation of mRNA and protein expression of multiple adhesion molecules, such as VCAM1, ICAM1, PECAM-1, VE-cadherin, E-Selectin and P-Selectin (Fig. 6A and B). In addition, after the transfection of sh-SLC12A2 into HG-treated cells, the expression levels of these factors displayed a downward trend. Except for

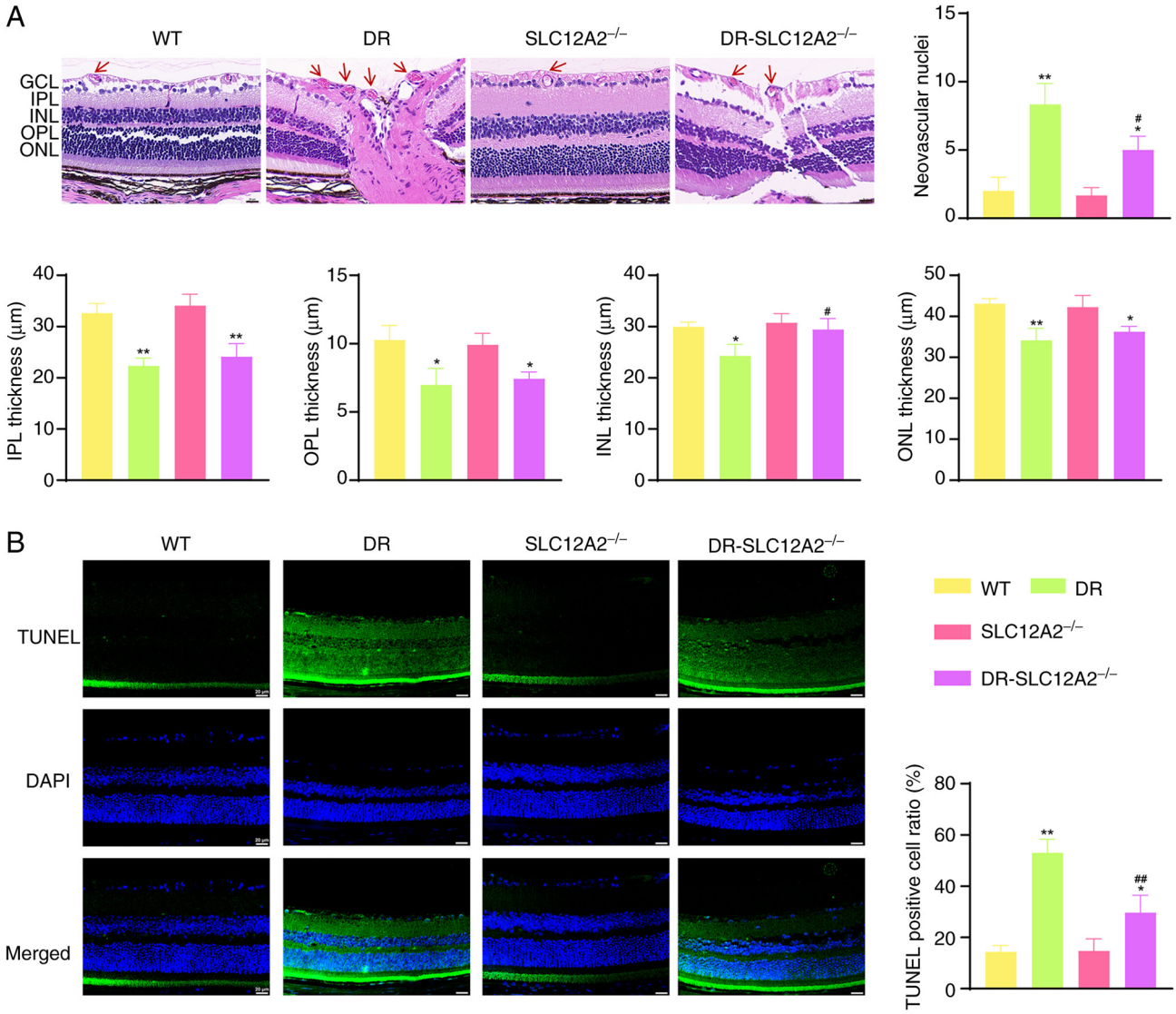

Figure 8. SLC12A2 deficiency inhibits retinal structural damage in streptozotocin-induced diabetic mice. (A) Representative H&E-stained images and retinal thickness measurements in each group (magnification, x40). The red arrow represents neovascular nuclei. (B) Representative TUNEL assay images in each group (magnification, x40). Results are expressed as the mean ± SD (n= 10/group). *P<0.05 and **P<0.01 vs. the WT group; $^{\#}$P<0.05 and $^{\#\#}$P<0.01 vs. the DR group. TUNEL, terminal deoxynucleotidyl transferase dUTP nick-end labeling; GCL, ganglion cell layer; IPL, inner plexiform layer; INL, inner nuclear layer; OPL, outer plexiform layer; ONL, outer nuclear layer; WT, wild-type; DR, diabetic retinopathy.

PECAM-1 and VE-cadherin, the expression changes of the other molecules showed statistical differences. Collectively, these results suggested that SLC12A2 knockdown inhibited the enhanced expression of adhesion-related molecules induced by HG stimulation.

SLC12A2 deficiency ameliorates hyperglycemic and inflammatory effects in STZ-induced diabetic mice. Based on these results, SLC12A2 may be a promising target for protecting retinal cells from hyperglycemic damage. Hence, the association between SLC12A2 and pathological changes in DR was evaluated by using an *in vivo* gene knockout. First, RT-qPCR and western blot results revealed that SLC12A2 expression levels in SLC12A2$^{-/-}$ mice were significantly reduced compared with those in WT mice, confirming the successful construction of the SLC12A2-KO model (Fig. S1A and B). In addition, there were no significant differences in body weight, serum lipid concentrations, or HbA1c levels between WT and SLC12A2$^{-/-}$ mice. A total of 7 days after STZ injection, DR and DR-SLC12A2$^{-/-}$ mice displayed increased body weight and blood glucose levels compared with those in control groups (WT and SLC12A2$^{-/-}$), indicating that the mice developed diabetes. Importantly, blood glucose levels, TG, TC and HbA1c levels were significantly lower in the DR-SLC12A2$^{-/-}$ group compared with the DR group (Fig. 7A-C). The secretion levels of inflammatory factors in mouse serum were also measured via ELISA. Results revealed that the diabetic mice had significantly elevated levels of inflammatory and angiogenic factors, including VEGF, IL-1β, IL-6 and TNF-α. However, SLC12A2 deficiency reduced the secretion of proinflammatory factors in diabetic mice (Fig. 7D). These data further confirmed that SLC12A2 may improve DR by controlling blood glucose levels and suppressing inflammatory responses.

SLC12A2 deficiency inhibits retinal structural damage in STZ-induced diabetic mice. Following, H&E staining was

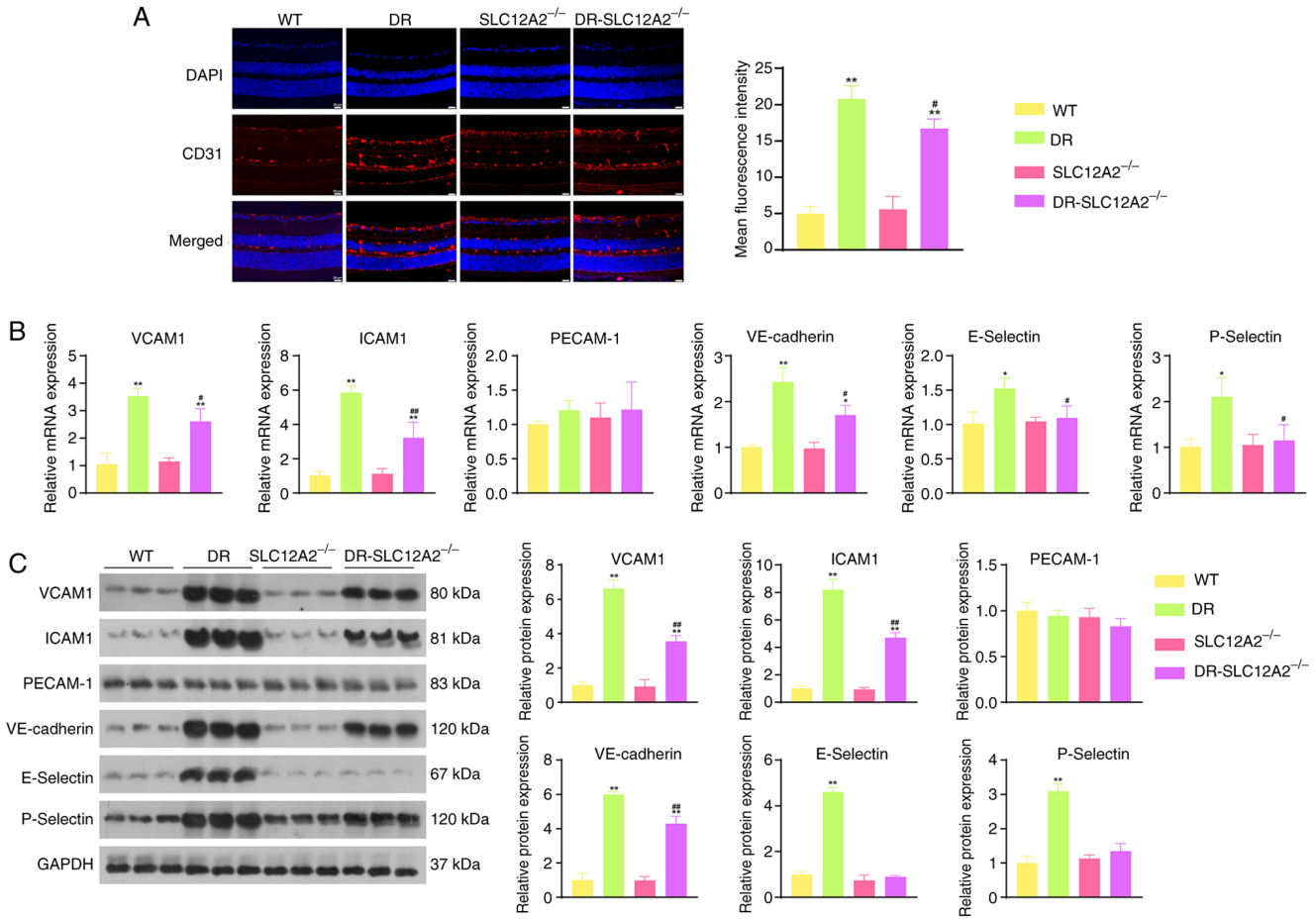

Figure 9. SLC12A2 deficiency suppresses adhesion molecule expression in streptozotocin-induced diabetic mice. (A) Immunofluorescence images of CD31 (magnification, x40). (B and C) Expression of VCAM1, ICAM1, PECAM-1, VE-cadherin, E-Selectin and P-Selectin determined by reverse transcription-quantitative PCR and western blotting. Results are expressed as the mean ± SD (n=10/group). *P<0.05 and **P<0.01 vs. the WT group; $^{\#}$P<0.05 and $^{\#\#}$P<0.01 vs. the DR group. VCAM1, vascular cell adhesion molecule-1; ICAM1, intercellular adhesion molecule-1; PECAM-1, platelet endothelial cell adhesion molecule-1; VE, vascular endothelial; WT, wild-type; DR, diabetic retinopathy.

utilized to observe pathological changes in the retina (Fig. 8A). Results showed that the structure of the retinal layers in the WT group was clear, with the INL and ONL cells arranged in an orderly and tight manner. However, in the DR group, a neovascularized cavity was observed in the retina (red arrows), and its structure was markedly dilated and vacuolated. The GCL appeared to be fractured, and the cells in each layer were loosely arranged, indicating significant pathological changes in the retinal tissue. Notably, the structure and shape of the retina in the DR-SLC12A2$^{-/-}$ mice were clearly improved compared with those in DR mice. Furthermore, statistical analysis indicated that DR mice had an increased number of neovascular nuclei, but a significantly thinner INL than WT mice. SLC12A2 knockout significantly ameliorated these pathological impairments in diabetic mice, as evidenced by increased retinal thickness and a reduced number of neovascular nuclei. Subsequently, TUNEL was employed to explore the effect of SLC12A2 deficiency on retinal apoptosis in the diabetic state (Fig. 8B). The proportion of TUNEL-positive cells in the DR group was significantly higher than that in the WT group. As expected, SLC12A2 deficiency markedly reduced the rate of apoptosis. Collectively, these results suggested that SLC12A2 deficiency has a significant protective effect against diabetic retinal damage.

SLC12A2 deficiency suppresses cell adhesion molecules expression in STZ-induced diabetic mice. Considering that the protective effect of the SLC12A2 knockdown in endothelial cells was achieved by suppressing the expression of adhesion-related molecules, this finding was further validated *in vivo*. As demonstrated in Fig. 9A, the protein expression level of CD31 in the retinas of STZ-triggered DR mice significantly increased, while SLC12A2 knockout suppressed its expression. Besides, the mRNA and protein expression levels of multiple adhesion molecules, including VCAM1, ICAM1, and VE-cadherin, were significantly increased in the retinas of DR mice compared with those of WT mice. SLC12A2 knockout showed the opposite changes in the expression of these genes (Fig. 9B and C). Collectively, the aforementioned results suggested that SLC12A2 deficiency alleviates the pathological changes in DR by inhibiting the expression of cell adhesion-related molecules.

Discussion

Anti-VEGF approaches play a prominent role in the treatment of DR (41). However, treating patients who respond poorly to this approach remains a clinical challenge, and therapeutic agents against novel pathological targets may be required. In

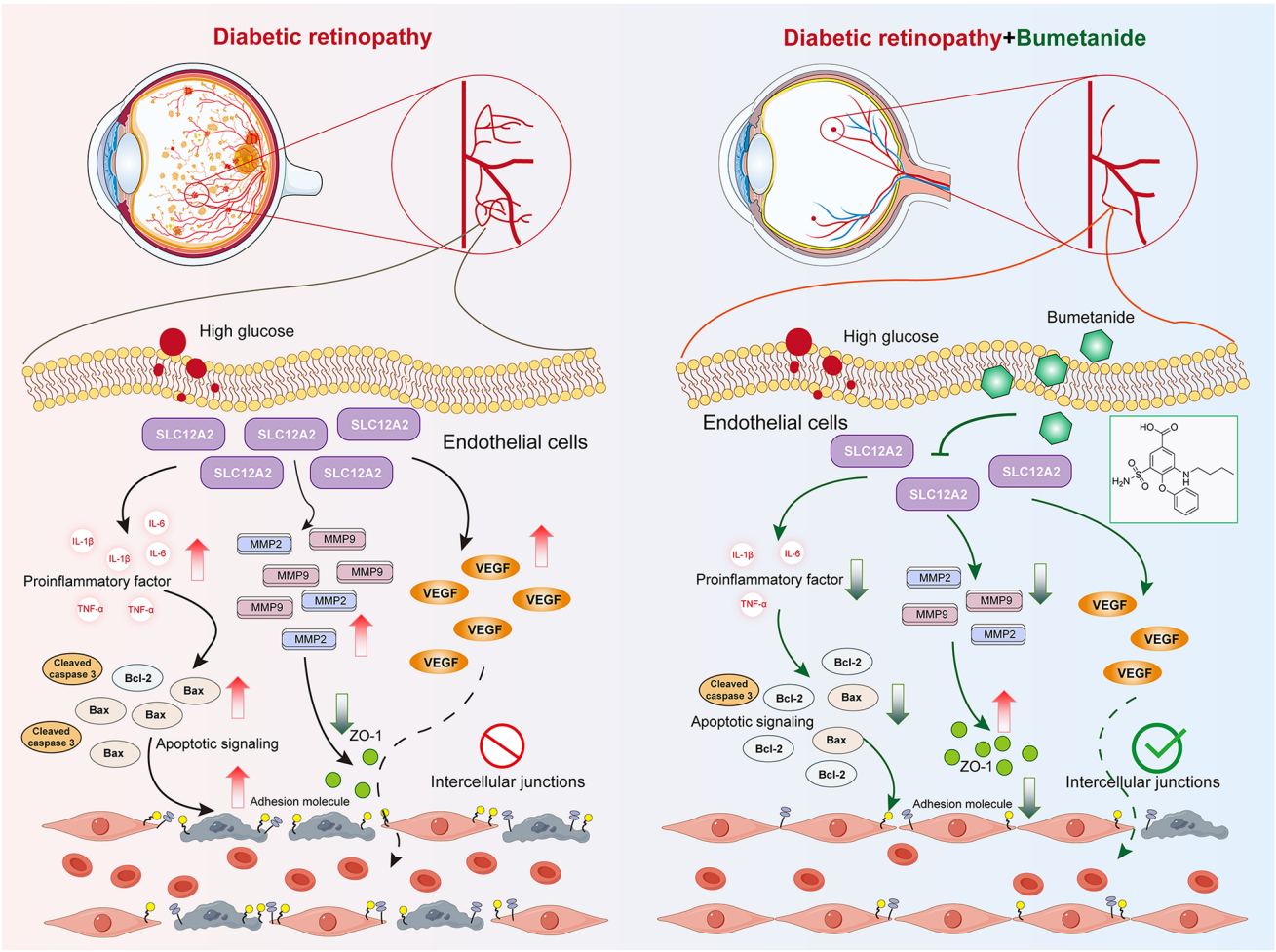

Figure 10. Molecular mechanisms of bumetanide treatment for DR. Bumetanide can directly inhibit the expression of SLC12A2, thereby effectively alleviating the pathological changes of DR by reducing inflammatory responses, inhibiting the expression of adhesion molecules, decreasing cell apoptosis, and enhancing the integrity of the blood-retinal barrier. DR, diabetic retinopathy.

the present study, scRNA-seq analysis revealed that DR was composed of six cell types, and SLC12A2 was predominantly expressed in endothelial cells. Endothelial cell markers were significantly involved in angiogenesis regulation and adhesion molecule-related biological functions. Importantly, it was found that bumetanide and its drug target SLC12A2 inhibited abnormal apoptosis and angiogenesis in an *in vitro* DR model. It was further demonstrated *in vivo* that SLC12A2 deficiency suppressed hyperglycemia and maintained normal retinal anatomy in diabetic mice, thereby preventing the development of DR. Notably, the underlying vascular protective mechanism of SLC12A2 may involve the inhibition of cell adhesion molecules, leading to a reduction in apoptotic and inflammatory events (Fig. 10). These findings suggested that SLC12A2is a promising biomarker for the development of DR-targeted drugs.

Bumetanide modulates retinal function by reducing retinal swelling and damage (42). This mechanism involves competition with Cl^- for the second chloride-binding site, which exerts the functions of inhibiting NKCC1 (SLC12A2) (43). In the present study, for the first time to the best of the authors' knowledge, the effect of bumetanide on HG-treated RRMECs was observed. Bumetanide significantly suppressed the expression of SLC12A2 and SLC12A4 in HG-exposed endothelial cells (RRMECs). Endothelial cells, the innermost layer of blood vessels, are the primary targets of damage under HG conditions (44). Similar to previous results (8), in the HG-induced RRMECs injury model, bumetanide suppressed the expression of apoptotic proteins (cleaved-caspase 3 and Bax) while increasing the levels of anti-apoptotic proteins (BCL-2), thus reducing the number of apoptotic cells. Importantly, inflammatory molecules and neovascularization play crucial roles in the pathogenesis and progression of DR (45-47). It was observed that bumetanide treatment significantly reduced the expression of inflammatory factors (TNF-α and IL-1β) and VEGF in HG-stimulated cells, consistent with findings reported by Guzel *et al* (48). Taken together, bumetanide ameliorates diabetes-induced retinal inflammation and vascular dysfunction, thereby attenuating DR progression.

The protective effects of bumetanide were inspiring and thus its underlying mechanisms were investigated. Two pharmacological targets of bumetanide were explored. Bioinformatics analysis of scRNA-seq and RNA-seq data revealed that SLC12A2 was predominantly highly expressed in endothelial cells, whereas SLC12A4 was primarily localized in fibroblasts. Microvascular dysfunction is a central pathogenic hallmark of DR. As a fundamental structural and

functional unit of the retinal blood vessels, endothelial cell stability is essential for maintaining vascular integrity. In the early stages of DR, hyperglycemic stimulation induces apoptosis, phenotypic alterations, and enhanced migratory capacity in retinal endothelial cells, consequently leading to increased vascular permeability and pathological neovascularization. These changes ultimately contribute to the development of microaneurysms, fluid leakage and tissue damage (49,50). Furthermore, as DR progresses, dysfunctional endothelial cells promote excessive accumulation of extracellular matrix proteins in the retina and activate fibroblast proliferation (51). Massive proliferation of fibroblasts triggers retinal fibrosis, leading to severe visual impairments such as tractional retinal detachment (52). Taken together, endothelial cell injury may represent a critical early event in DR, allowing the invasion of pathogenic factors that occur before other events (53). Therefore, the protection of endothelial cells is a potential therapeutic target for early-stage DR interventions. However, current treatment modalities primarily address advanced DR, and the ability to restore impaired vision remains limited (54). Based on this evidence, SLC12A2 was selected, which is highly expressed in endothelial cells, as the target for functional experiments.

As expected, in HG-treated RRMECs, SLC12A2 knockdown promoted cell proliferation, while attenuating cell migration and pathological angiogenesis. These results suggested that SLC12A2 knockdown attenuates cell damage in DR, which is consistent with the results of a previous study (35). The role of inflammatory processes in the pathological changes associated with DR has received extensive attention. There is crosstalk between inflammation and neovascularization in the pathogenesis of DR, and inhibition of inflammation may facilitate the control of retinal angiogenesis (38). In the present study, SLC12A2 knockdown markedly reduced the release of inflammatory factors in HG-treated RRMECs, such as VEGF, IL-1β, IL-6 and TNF-α. The internal BRB is a highly selective endothelial barrier that maintains tissue homeostasis by regulating permeability and molecular transport between the circulatory system and the neural retina (55). In patients with DR, inner BRB (iBRB) disruption leads to retinal neurodegeneration and vision loss (56). Therefore, the effects of SLC12A2 knockdown were examined on the expression of core functional proteins essential for iBRB integrity. Results showed that SLC12A2 knockdown maintained the integrity of the iBRB by upregulating ZO-1 and downregulating MMP2/MMP9. Reportedly, reduced ZO-1 levels disrupt tight junctions in endothelial cells, leading to dysfunction of the endothelial barrier (57). Activation of MMPs, particularly MMP2 and MMP9, represents an early event in DR that induces mitochondrial damage and promotes retinal apoptosis in vascular cells (pericytes and endothelial cells) (28,58). Similarly, SLC12A2 deficiency alleviated the progression of DR *in vivo* by improving retinal thickness and pathological changes (inflammation and angiogenesis) in STZ-induced diabetic mice. Consequently, SLC12A2 knockdown may exert a protective effect against DR by preventing iBRB breakdown through suppression of proinflammatory factors and VEGF expression.

Subsequently, it was found that endothelial cell markers were primarily involved in pathways related to angiogenesis and cell adhesion. The upregulation of adhesion molecules is a critical step in the pathogenesis of DR. Hyperglycemia-induced proinflammatory cytokines secrete intercellular adhesion molecules such as ICAM-1 and VCAM-1, which mediate leukocyte-endothelial cell interactions to promote leukocyte recruitment, facilitating a persistent inflammatory response, thereby leading to increased retinal capillary permeability and stimulating pathological retinal neovascularization (59-61). Therefore, observing the changes in adhesion molecules caused by SLC12A2 knockdown is important. It was found that SLC12A2 knockdown significantly rescued the HG-induced enhanced expression of adhesion factors, including VCAM1, ICAM1, E-Selectin and P-Selectin. VCAM1 promotes adhesion between leukocytes and vascular endothelial cells, which is positively correlated with the severity of DR (62). Indeed, a reduction in VCAM1 has been reported in DR remission (32). ICAM1 plays a similar role and its expression is inhibited by DR therapeutic drugs such as finerenone (63). E-Selectin is present in activated endothelial cells and plays an important role in leukocyte recruitment to inflammatory areas (64). Controlling blood glucose reduces E-Selectin levels, which may play a role in preventing DR (65). P-Selectin is also involved in leukocyte recruitment, and its high levels are potentially associated with DR (66). Taken together, the inhibition of SLC12A2 alleviates DR-associated pathological symptoms, indicating that SLC12A2 may be a valuable therapeutic candidate against DR.

To the best of the authors' knowledge, this is the first study to elucidate the protective role of bumetanide against endothelial cell injury in DR and its specific molecular mechanisms. However, the limitations of the present study warrant further investigation. First, it was concluded that bumetanide prevents DR progression by downregulating SLC12A2 to reduce inflammatory factors, growth factors, and adhesion molecules in endothelial cells. Nevertheless, the specific downstream targets of SLC12A2 remain unknown. Second, the current results have only been validated in HG-induced RRMECs and STZ-induced diabetic mouse models, which may not fully replicate the complex pathological environment of human DR. Third, although focus was mainly addressed on the regulatory role of SLC12A2 in DR, whether SLC12A4, another pharmacological target of bumetanide, also exerts a similar effect remains unexplored. Therefore, more comprehensive and in-depth studies on endothelially expressed SLC12A2 and SLC12A4 in DR are warranted.

In summary, the current data indicate that SLC12A2, a key pharmacological target of bumetanide, is effective in alleviating pathological alterations in DR, including the attenuation of the inflammatory response, suppression of adhesion molecule expression, reduction of cell apoptosis, and enhancement of BRB integrity. The present study is the first to demonstrate the protective effects of bumetanide against DR, suggesting that targeting SLC12A2 may represent a promising preventive or therapeutic strategy against DR.

Acknowledgements

Not applicable.

Funding

No funding was received.

Availability of data and materials

The data generated in the present study may be requested from the corresponding author.

Authors' contributions

YZ and HY conceived and designed the research. YZ, YH, DH and ZL acquired data. YH, DH, XW, HY, QX and MN analyzed and interpreted data. YZ, TX, XW, HY, QX and MN performed statistical analysis. YZ and YH drafted the manuscript. HY, XW and QX revised the manuscript for important intellectual content. All authors confirm the authenticity of all the raw data. All authors read and approved the final version of the manuscript.

Ethics approval and consent to participate

Animal procedures were performed in compliance with the ARRIVE guidelines and were approved from the Ethics Committee of the Experimental Animal Center of Yangzhou University (approval no. 202410027; Yangzhou, China).

Patient consent for publication

Not applicable.

Competing interests

The authors declare that they have no competing interests.

References

1. Tan TE and Wong TY: Diabetic retinopathy: Looking forward to 2030. Front Endocrinol (Lausanne) 13: 1077669, 2022.
2. Teo ZL, Tham YC, Yu M, Chee M, Rim TH, Cheung N, Bikbov MM, Wang YX, Tang Y, Lu Y, *et al*: Global prevalence of diabetic retinopathy and projection of burden through 2045: Systematic review and meta-analysis. Ophthalmology 128: 1580-1591, 2021.
3. Himasa FI, Singhal M, Ojha A and Kumar B: Prospective for diagnosis and treatment of diabetic retinopathy. Curr Pharm Des 28: 560-569, 2022.
4. Ren J, Zhang S, Pan Y, Jin M, Li J, Luo Y, Sun X and Li G: Diabetic retinopathy: Involved cells, biomarkers, and treatments. Front Pharmacol 13: 953691, 2022.
5. Kaushik V, Gessa L, Kumar N and Fernandes H: Towards a new biomarker for diabetic retinopathy: Exploring RBP3 structure and retinoids binding for functional imaging of eyes in vivo. Int J Mol Sci 24: 4408, 2023.
6. Lam TI, Anderson SE, Glaser N and O'donnell M E: Bumetanide reduces cerebral edema formation in rats with diabetic ketoacidosis. Diabetes 54: 510-516, 2005.
7. Guzel S, Cai CL, Ahmad T, Quan M, Valencia GB, Aranda JV and Beharry KD: Bumetanide suppression of angiogenesis in a rat model of Oxygen-induced retinopathy. Int J Mol Sci 21: 987, 2020.
8. Chen C, Fan P, Zhang L, Xue K, Hu J, Huang J, Lu W, Xu J, Xu S, Qiu G, *et al*: Bumetanide rescues Aquaporin-4 depolarization via suppressing β-dystroglycan cleavage and provides neuroprotection in rat retinal ischemia-reperfusion injury. Neuroscience 510: 95-108, 2022.
9. Navas A, Jannus F, Fernández B, Cepeda J, Medina O'Donnell M, Díaz-Ruiz L, Sánchez-González C, Llopis J, Seco JM, Rufino-Palomares E, *et al*: Designing Single-molecule magnets as drugs with dual Anti-inflammatory and anti-diabetic effects. Int J Mol Sci 21: 3146, 2020.
10. Hampel P, Römermann K, Gailus B, Johne M, Gericke B, Kaczmarek E and Löscher W: Effects of the NKCC1 inhibitors bumetanide, azosemide, and torasemide alone or in combination with phenobarbital on seizure threshold in epileptic and nonepileptic mice. Neuropharmacology 185: 108449, 2021.
11. Rivera A, Nasburg JA, Shim H, Shmukler BE, Kitten J, Wohlgemuth JG, Dlott JS, Snyder LM, Brugnara C, Wulff H and Alper SL: The erythroid K-Cl cotransport inhibitor [(dihydroindenyl)oxy]acetic acid blocks erythroid Ca2+-activated K+ channel KCNN4. Am J Physiol Cell Physiol 323: C694-C705, 2022.
12. Tang F, Barbacioru C, Wang Y, Nordman E, Lee C, Xu N, Wang X, Bodeau J, Tuch BB, Siddiqui A, *et al*: mRNA-Seq whole-transcriptome analysis of a single cell. Nat Methods 6: 377-382, 2009.
13. Van Hove I, De Groef L, Boeckx B, Modave E, Hu TT, Beets K, Etienne I, Van Bergen T, Lambrechts D, Moons L, *et al*: Single-cell transcriptome analysis of the Akimba mouse retina reveals cell-type-specific insights into the pathobiology of diabetic retinopathy. Diabetologia 63: 2235-2248, 2020.
14. Zhang X, Zhang F and Xu X: Single-cell RNA sequencing in exploring the pathogenesis of diabetic retinopathy. Clin Transl Med 14: e1751, 2024.
15. Sun L, Wang R, Hu G, Liu H, Lv K, Duan Y, Shen N, Wu J, Hu J, Liu Y, *et al*: Single cell RNA sequencing (scRNA-Seq) deciphering pathological alterations in streptozotocin-induced diabetic retinas. Exp Eye Res 210: 108718, 2021.
16. Liu K, Gao X, Hu C, Gui Y, Gui S, Ni Q, Tao L and Jiang Z: Capsaicin ameliorates diabetic retinopathy by inhibiting poldip2-induced oxidative stress. Redox Biol 56: 102460, 2022.
17. Theocharidis G, Thomas BE, Sarkar D, Mumme HL, Pilcher WJR, Dwivedi B, Sandoval-Schaefer T, Sîrbulescu RF, Kafanas A, Mezghani I, *et al*: Single cell transcriptomic landscape of diabetic foot ulcers. Nat Commun 13: 181, 2022.
18. Liao D, Fan W, Li N, Li R, Wang X, Liu J, Wang H and Hou S: A single cell atlas of circulating immune cells involved in diabetic retinopathy. iScience 27: 109003, 2024.
19. Hu Z, Mao X, Chen M, Wu X, Zhu T, Liu Y, Zhang Z, Fan W, Xie P, Yuan S and Liu Q: Single-cell transcriptomics reveals novel role of microglia in fibrovascular membrane of proliferative diabetic retinopathy. Diabetes 71: 762-773, 2022.
20. Xiang ZY, Chen SL, Qin XR, Lin SL, Xu Y, Lu LN and Zou HD: Changes and related factors of blood CCN1 levels in diabetic patients. Front Endocrinol (Lausanne) 14: 1131993, 2023.
21. Hui Z, Chen YM, Gong WK, Lai JB, Yao BB, Zhao ZJ, Lu QK, Ye K, Ji LD and Xu J: Shared and specific biological signalling pathways for diabetic retinopathy, peripheral neuropathy and nephropathy by high-throughput sequencing analysis. Diab Vasc Dis Res 19: 14791641221122918, 2022.
22. Gui F, You Z, Fu S, Wu H and Zhang Y: Endothelial dysfunction in diabetic retinopathy. Front Endocrinol (Lausanne) 11: 591, 2020.
23. Kaur G, Song Y, Xia K, Mccarthy K, Zhang F, Linhardt RJ and Harris NR: Effect of high glucose on glycosaminoglycans in cultured retinal endothelial cells and rat retina. Glycobiology 32: 720-734, 2022.
24. Shi J, Lv H, Tang C, Li Y, Huang J and Zhang H: Mangiferin inhibits cell migration and angiogenesis via PI3K/AKT/mTOR signaling in high glucose- and hypoxia-induced RRCECs. Mol Med Rep 23: 473, 2021.
25. Justus CR, Marie MA, Sanderlin EJ and Yang LV: Transwell in vitro cell migration and invasion assays. Methods Mol Biol 2644: 349-359, 2023.
26. Lin Y, Luo G, Liu Q, Yang R, Sol Reinach P and Yan D: METTL3-mediated RNA m6A modification regulates the angiogenic behaviors of retinal endothelial cells by methylating MMP2 and TIE2. Invest Ophthalmol Vis Sci 64: 18, 2023.
27. Li J, Lu X, Wei L, Ye D, Lin J, Tang X, Cui K, Yu S, Xu Y and Liang X: PHD2 attenuates high-glucose-induced blood retinal barrier breakdown in human retinal microvascular endothelial cells by regulating the Hif-1α/VEGF pathway. Inflamm Res 71: 69-79, 2021.
28. Giebel SJ, Menicucci G, Mcguire PG and Das A: Matrix metalloproteinases in early diabetic retinopathy and their role in alteration of the blood-retinal barrier. Lab Invest 85: 597-607, 2005.
29. Huang Y, Wang Z, Ye B, Ma JH, Ji S, Sheng W, Ye S, Ou Y, Peng Y, Yang X, *et al*: Sodium butyrate ameliorates diabetic retinopathy in mice via the regulation of gut microbiota and related short-chain fatty acids. J Transl Med 21: 451, 2023.
30. Zhang L, Zhou X, Chen H, You L, Zhang T, Cheng M, Yao Y, Pan X and Yang X: Mulberry extract ameliorates T2DM-related symptoms via AMPK pathway in STZ-HFD-induced C57BL/6J mice. J Ethnopharmacol 313: 116475, 2023.
31. Wu L, Li J, Zhao F and Xiang Y: MiR-340-5p inhibits Müller cell activation and pro-inflammatory cytokine production by targeting BMP4 in experimental diabetic retinopathy. Cytokine 149: 155745, 2021.

32. Ai X, Yu P, Luo L, Sun J, Tao H, Wang X and Meng X: Berberis Dictyophylla F. inhibits angiogenesis and apoptosis of diabetic retinopathy via suppressing HIF-1α/VEGF/DLL-4/Notch-1 pathway. J Ethnopharmacol 296: 115453, 2022.
33. Kyrylkova K, Kyryachenko S, Leid M and Kioussi C: Detection of apoptosis by TUNEL assay. Methods Mol Biol 887: 41-47, 2012.
34. Hu L, Lv X, Li D, Zhang W, Ran G, Li Q and Hu J: The anti-angiogenesis role of FBXW7 in diabetic retinopathy by facilitating the ubiquitination degradation of c-Myc to orchestrate the HDAC2. J Cell Mol Med 25: 2190-2202, 2020.
35. Shao J, Bai Z, Zhang L and Zhang F: Ferrostatin-1 alleviates tissue and cell damage in diabetic retinopathy by improving the antioxidant capacity of the Xc-GPX4 system. Cell Death Discov 8: 426, 2022.
36. Livak KJ and Schmittgen TD: Analysis of relative gene expression data using real-time quantitative PCR and the 2(-Delta Delta C(T)) method. Methods 25: 402-408, 2001.
37. Simó R, Simó-Servat O, Bogdanov P and Hernández C: Diabetic retinopathy: Role of neurodegeneration and therapeutic perspectives. Asia Pac J Ophthalmol (Phila) 11: 160-167, 2022.
38. Kaštelan S, Orešković I, Bišćan F, Kaštelan H and Gverović Antunica A: Inflammatory and angiogenic biomarkers in diabetic retinopathy. Biochem Med (Zagreb) 30: 030502, 2020.
39. Gardner TW: Histamine, ZO-1 and increased blood-retinal barrier permeability in diabetic retinopathy. Trans Am Ophthalmol Soc 93: 583-621, 1995.
40. Blum A, Pastukh N, Socea D and Jabaly H: Levels of adhesion molecules in peripheral blood correlat with stages of diabetic retinopathy and may serve as bio markers for microvascular complications. Cytokine 106: 76-79, 2018.
41. Uludag G, Hassan M, Matsumiya W, Pham BH, Chea S, Trong Tuong Than N, Doan HL, Akhavanrezayat A, Halim MS, Do DV and Nguyen QD: Efficacy and safety of intravitreal anti-VEGF therapy in diabetic retinopathy: What we have learned and what should we learn further? Expert Opin Biol Ther 22: 1275-1291, 2022.
42. Crewther SG, Murphy MJ and Crewther DP: Potassium channel and NKCC cotransporter involvement in ocular refractive control mechanisms. PLoS One 3: e2839, 2008.
43. Russell JM: Sodium-potassium-chloride cotransport. Physiol Rev 80: 211-276, 2000.
44. Betts-Obregon BS, Vellanki S, Buikema J, Tsin AT and Wright K: Effect of glucose on retinal endothelial cell viability and VEGF secretion. HSOA J Cell Biol Cell Metabol 3: 008, 2016.
45. Uemura A, Fruttiger M, D'amore PA, De Falco S, Joussen AM, Sennlaub F, Brunck LR, Johnson KT, Lambrou GN, Rittenhouse KD and Langmann T: VEGFR1 signaling in retinal angiogenesis and microinflammation. Prog Retin Eye Res 84: 100954, 2021.
46. Tang L, Xu GT and Zhang JF: Inflammation in diabetic retinopathy: Possible roles in pathogenesis and potential implications for therapy. Neural Regen Res 18: 976-982, 2023.
47. Panda SP, Reddy PH, Gorla US and Prasanth D: Neuroinflammation and neovascularization in diabetic eye diseases (DEDs): Identification of potential pharmacotherapeutic targets. Mol Biol Rep 50: 1857-1869, 2022.
48. Guzel S, Cai CL, Aranda JV and Beharry KD: Dose response of bumetanide on aquaporins and angiogenesis biomarkers in human retinal endothelial cells exposed to intermittent hypoxia. Pharmaceuticals (Basel) 14: 967, 2021.
49. Yang S, Zhang J and Chen L: The cells involved in the pathological process of diabetic retinopathy. Biomed Pharmacother 132: 110818, 2020.
50. Rajendran S, Seetharaman S, Dharmarajan A and Kuppan K: Microvascular cells: A special focus on heterogeneity of pericytes in diabetes associated complications. Int J Biochem Cell Biol 134: 105971, 2021.
51. Abu El-Asrar AM, De Hertogh G, Van Den Eynde K, Alam K, Van Raemdonck K, Opdenakker G, Van Damme J, Geboes K and Struyf S: Myofibroblasts in proliferative diabetic retinopathy can originate from infiltrating fibrocytes and through endothelial-to-mesenchymal transition (EndoMT). Exp Eye Res 132: 179-189, 2015.
52. Tuleta I and Frangogiannis NG: Diabetic fibrosis. Biochim Biophys Acta Mol Basis Dis 1867: 166044, 2020.
53. Yao X, Zhao Z, Zhang W, Liu R, Ni T, Cui B, Lei Y, Du J, Ai D, Jiang H, *et al*: Specialized retinal endothelial cells modulate Blood-Retina barrier in diabetic retinopathy. Diabetes 73: 225-236, 2024.
54. Yamato M, Kato N, Yamada KI and Inoguchi T: The early pathogenesis of diabetic retinopathy and its attenuation by sodium-glucose transporter 2 inhibitors. Diabetes 73: 1153-1166, 2024.
55. O'Leary F and Campbell M: The blood-retina barrier in health and disease. FEBS J 290: 878-891, 2021.
56. Maurissen TL, Spielmann AJ, Schellenberg G, Bickle M, Vieira JR, Lai SY, Pavlou G, Fauser S, Westenskow PD, Kamm RD and Ragelle H: Modeling early pathophysiological phenotypes of diabetic retinopathy in a human inner blood-retinal barrier-on-a-chip. Nat Commun 15: 1372, 2024.
57. Wang N, Yao F, Xu W, Feng T, Li Z, Zhang Q, Wang W, Zhang X, Lei W, Zheng G, *et al*: The transcription factor Islet-1 regulates Diabetes-induced inner blood-retinal barrier disruption. Invest Ophthalmol Vis Sci 66: 8, 2025.
58. Kowluru RA, Zhong Q and Santos JM: Matrix metalloproteinases in diabetic retinopathy: Potential role of MMP-9. Expert Opin Investig Drugs 21: 797-805, 2012.
59. Qian HY, Wei XH and Huang JO: Inflammatory mechanisms in diabetic retinopathy: Pathogenic roles and therapeutic perspectives. Am J Transl Res 17: 6262-6274, 2025.
60. Joys S and Siddiqui K: Molecular and pathophysiological mechanisms of diabetic retinopathy in relation to adhesion molecules. Curr Diabetes Rev 15: 363-371, 2019.
61. Yue T, Shi Y, Luo S, Weng J, Wu Y and Zheng X: The role of inflammation in immune system of diabetic retinopathy: Molecular mechanisms, pathogenetic role and therapeutic implications. Front Immunol 13: 1055087, 2022.
62. Xu Y, Hou H and Zhao L: The role of VCAM-1 in diabetic retinopathy: A systematic review and meta-analysis. J Diabetes Complications 37: 108380, 2023.
63. Jerome JR, Deliyanti D, Suphapimol V, Kolkhof P and Wilkinson-Berka JL: Finerenone, a Non-steroidal mineralocorticoid receptor antagonist, reduces vascular injury and increases regulatory T-Cells: Studies in rodents with diabetic and neovascular retinopathy. Int J Mol Sci 24: 2334, 2023.
64. Borgström P, Hughes GK, Hansell P, Wolitsky BA and Sriramarao P: Leukocyte adhesion in angiogenic blood vessels. Role of E-selectin, P-selectin, and beta2 integrin in lymphotoxin-mediated leukocyte recruitment in tumor microvessels. J Clin Invest 99: 2246-2253, 1997.
65. Kasza M, Meleg J, Vardai J, Nagy B, Szalai E, Damjanovich J, Csutak A, Ujhelyi B and Nagy V: Plasma E-selectin levels can play a role in the development of diabetic retinopathy. Graefes Arch Clin Exp Ophthalmol 255: 25-30, 2017.
66. Penman A, Hoadley S, Wilson JG, Taylor HA, Chen CJ and Sobrin L: P-selectin plasma levels and genetic variant associated with diabetic retinopathy in african Americans. Am J Ophthalmol 159: 1152-1160.e2, 2015.